PNAS
www.pnas.org

Supplementary Information for

Real-time detection of response regulator phosphorylation dynamics in live bacteria

Ryan J. Butcher[a], Jeffrey J. Tabor[a,b]

[a]Department of Bioengineering, Rice University, Houston, TX 77005;

[b]Department of Biosciences, Rice University, Houston, TX 77005;

Email: jeff.tabor@rice.edu

This PDF file includes:

Supplementary Information Text

SI Text 1: Fluorescence anisotropy data processing.

We found that mNG expression level, light scattering by bacterial cells, and changes in sample volume during experiments affect measured anisotropy values of bacterial cultures. In this section, we describe control experiments we performed to characterize these effects and compensate for them in our data.

Correction for anisotropy changes that occur as a function of mNG expression level

Anisotropy (*r*) should decrease with bacterial culture density due to inherent light-scattering (1) but remain constant for mNG regardless of expression level, due to the highly monomeric nature of mNG (2). However, we found that anisotropy signal varies with mNG expression level, which we quantify as total fluorescence intensity (the denominator term in **Eqn. 1, Fig. S1A**). We observe a clear trend where mNG and mNG-mNG expression samples converge to different *r* values at high total fluorescence levels, but *r* proportionally decreases at lower expression levels. The anisotropy of autofluorescent *E. coli* lacking *mNG* (BW29658) is in line with this trend (**Fig. S1A**). By normalizing the *r* values of both sets of samples to their respective convergent *r* value at high fluorescence, we find a common trendline based on a power function to describe the relationship between *r* and total fluorescence intensity for both mNG and mNG-mNG (**Fig. S1B**). Because *r* is a ratiometric value depending on all sources of fluorescence and light scattering within the sample, the contribution of bacterial cells to the signal becomes negligible at higher mNG expression levels. Anisotropy (*r*) becomes independent of total fluorescence after correcting the data via the aforementioned trendline (**Fig. S1C**). Finally, at extremely low total fluorescence values (< 5,000 a.u.), we observe substantial signal degradation due to noise. Thus, we exclude samples with fluorescence values below this threshold (**Fig. S1a-c**).

Correction for anisotropy changes that occur due to experiment duration and sample volume

We observed that *r* decreases over relatively long timescales (1 hour) in mNG or mNG-mNG expressing cultures induced at constant levels (**Fig. S2A**). Using fluorescence microscopy (**Methods**), we found that intracellular mNG (or mNG-mNG) concentration also decreases slightly over the course of this experiment. This long time-scale reduction in mNG protein levels is likely due differences between our pre-incubation and experimental incubation conditions, such as a lack of constant shaking while inside the plate reader (**Methods**). Furthermore, because the bacteria are actively growing, the density of each culture increases over the course of the experiment. These two processes decrease *r*, as explained above. To correct for this drift, we normalize each anisotropy time course to the mean of the first two data points and fit the subsequent data points to a second-order polynomial (**Fig. S2B**), and then fit the generated parameters based on mNG fluorescence intensity (**Fig. S2C-D**). The constant term (coefficient *c*, **Fig. S2E**) is explained in the following paragraph.

To stimulate SHKs, we add ligands dissolved in M9 media to experimental cultures. In doing so, we increase sample volume from 180 to 200 μL. If there is no relevant ligand (as in this mNG-only experiments), we simply add M9 to cultures expressing monomeric or dimeric mNG to keep experimental conditions consistent. Addition of the 20 μL of M9 creates a discontinuity in our measured anisotropy values that persists for the duration of the experiment (**Fig. S2B**). This discontinuity arises because the slightly increased sample pathlength created by addition of the 20 μL of M9 increases light scattering. Much like how samples with lower mNG fluorescence are increasingly affected by bacterial light scattering, the discontinuity is greater at lower mNG fluorescence levels (**Fig. S2E**). A predicted drift function based on the three terms in **Fig. S2C-E** is then subtracted from the observed anisotropy values to correct for anisotropy value drift during our experiments (**Fig. S2F**).

Impact of molecular rotation on fluorescence anisotropy

Molecular rotation during the fluorescence lifetime of a fluorophore will decrease the measured fluorescence anisotropy. However, mNG is a relatively large molecule with a relatively

short fluorescence lifetime (3), so the effects of molecular rotation on fluorescence anisotropy are expected to be minimal (2). In a previous study on GFP dimerization, researchers utilized time-resolved fluorescence measurements to isolate the homoFRET component of the dimerization-induced anisotropy signal, improving the signal magnitude by roughly 10% (4). Therefore, the effects of molecular rotation are minimal in this case.

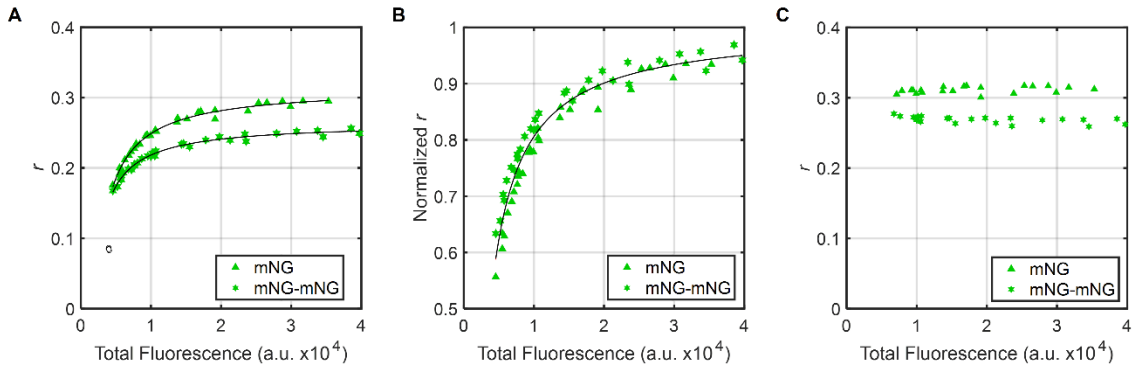

Figure S1. Compensating for total fluorescence of the bacterial culture. **A.** Uncorrected anisotropy values for cultures expressing varied amounts of mNG or mNG-mNG. Data represent 3 biological replicates treated with 10 aTc induction conditions: 4, 4.25, 4.5 4.75, 5, 6, 7, 8, 10, and 12 ng/mL. The unfilled circles indicate the anisotropy and total fluorescence of six single-day biological replicates of *E. coli* cultures lacking any *mNG* gene. Low variance gives the appearance of a single circle. **B.** Data from panel A normalized to the respective convergent *r* values of the two datasets (mNG: 0.3156; mNG-mNG: 0.2645), generating a common correction curve based on a power function (black line). **C.** Corrected anisotropy values for cultures expressing monomeric or dimeric mNG (7 aTc induction conditions: 4.75, 5, 6, 7, 8, 10, and 12 ng/mL).

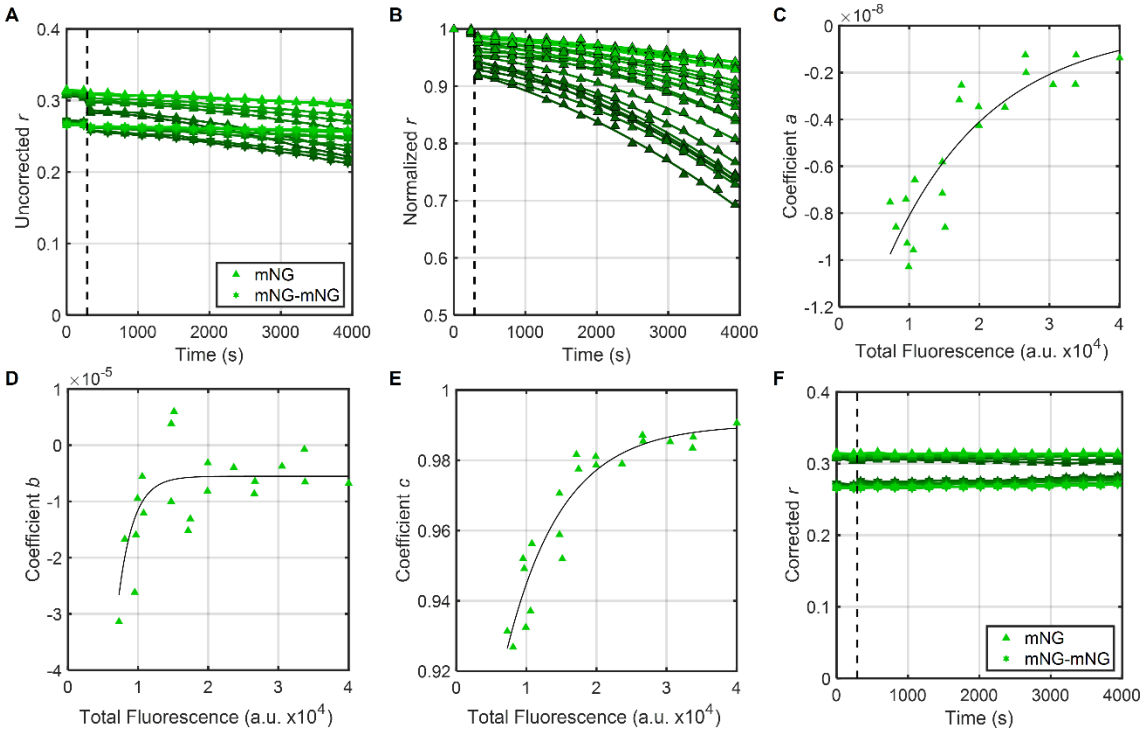

Figure S2. Compensating for anisotropy drift. A. Observed anisotropy signal over time for bacteria expressing mNG or mNG-mNG with total fluorescence corrections applied as in **Fig. S1**. Data are the mean of three biological replicates treated with 7 aTc induction conditions: 4.75, 5, 6, 7, 8, 10, and 12 ng/mL, where higher concentrations of aTc are represented by darker shades of green. **B**. Anisotropy time courses from panel A normalized to the respective initial *r* values, fitted to the second order polynomial $\boldsymbol{y = ax^2 + bx + c}$. **C-E**. Polynomial coefficients exponentially fitted to total fluorescence. Coefficient *c* (panel E) describes the immediate change in observed anisotropy after volume addition. **F**. Corrected anisotropy time courses from panel A. Throughout the main text and remaining supplementary information, we refer to corrected *r* values as *r* values.

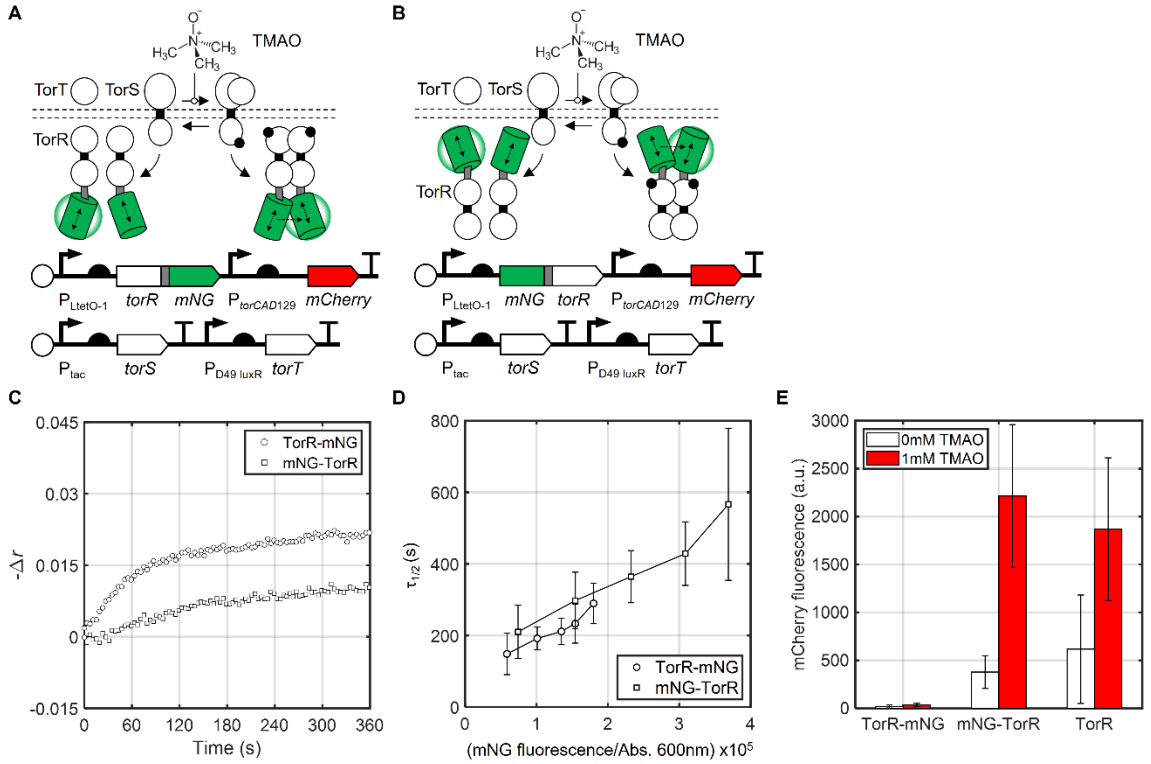

Figure S3. mNG probe placement does not affect TorR dimerization kinetics, but does affect TorR transcriptional regulatory activity. Strains engineered to express aTc-inducible (**A**) TorR-mNG or (**B**) mNG-TorR, alongside IPTG-inducible TorS, AHL-inducible TorT, and *mCherry* from the TorR-activated promoter $P_{torCAD129}$. **C.** Anisotropy changes over time after TMAO addition (time zero) for each strain. 4.8 ng/mL aTc, 32 µM IPTG, and 1 µM AHL were added. Data points represent the mean of three biological replicates measured on separate days. **D.** Triplicate-averaged $\tau_{1/2}$ values for both strains. The mNG-tagged TorR was induced to different expression levels as in **Fig. 2D**. mNG-tagged TorR expression level is plotted as culture mNG fluorescence normalized to culture density (**Methods**). aTc levels were varied between 4.8 and 12 ng/mL, IPTG was supplied at 100 µM, and AHL was added at 1 µM. **E.** mCherry fluorescence in the absence and presence of TMAO for the TorR-mNG and mNG-TorR expression strains and strain expressing a WT TorR control. Cultures were induced as in panels C and D. Data are reported as the population mean of segmented-cell median pixel intensities imaged via microscopy (**Methods**). Error bars indicate population standard deviation of segmented-cell median pixel intensities. Roughly 300 cells from two biological replicate populations were imaged for each condition.

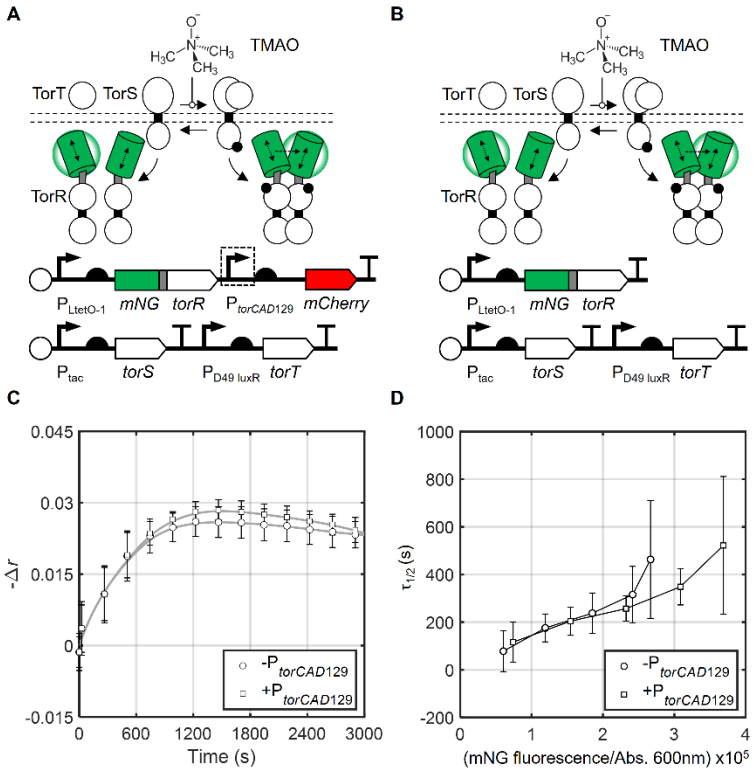

Figure S4: Supplemental TorR target promoters do not affect mNG-TorR dimerization rate. **A.** Engineered strain for inducible mNG-TorR expression from a ColE1 plasmid backbone with the TorR target promoter $P_{torCAD129}$ encoded on the plasmid (boxed). ColE1 plasmids are present at approximately 18 copies per cell (5). **B**. Control strain without $P_{torCAD129}$ present on the plasmid. Plasmids are transformed into *E. coli* BW29855 (Δ*torS-torD*) as in all other TorSR experiments. The native P_{torR} and P_{torCAD} promoters are absent from the genome in this strain. The remaining TorR binding sites (*hdeAB*, *gadAX*, *tnaC*, *tnaAB*) are present in the genome. **C.** Anisotropy change over time after TMAO addition (time zero) for cultures with or without $P_{torCAD129}$ present on the plasmid. TorS induced with 100 µM IPTG, TorR-mNG and TorT induced with 6.0 ng/mL aTc and 1 µM AHL, respectively). Smoothing splines were fitted to either data set to guide the eye. **D.** $\tau_{1/2}$ values of mNG-TorR dimerization at different mNG-TorR expression levels in the presence or absence of plasmid-borne $P_{torCAD129}$**.** aTc was varied between 4.8 and 12 ng/mL as in **Fig. 2D,** TorS induced with 100 µM IPTG, TorT induced with 1 µM AHL. Data represents the mean and standard deviation of three replicates of each condition collected on separate days.

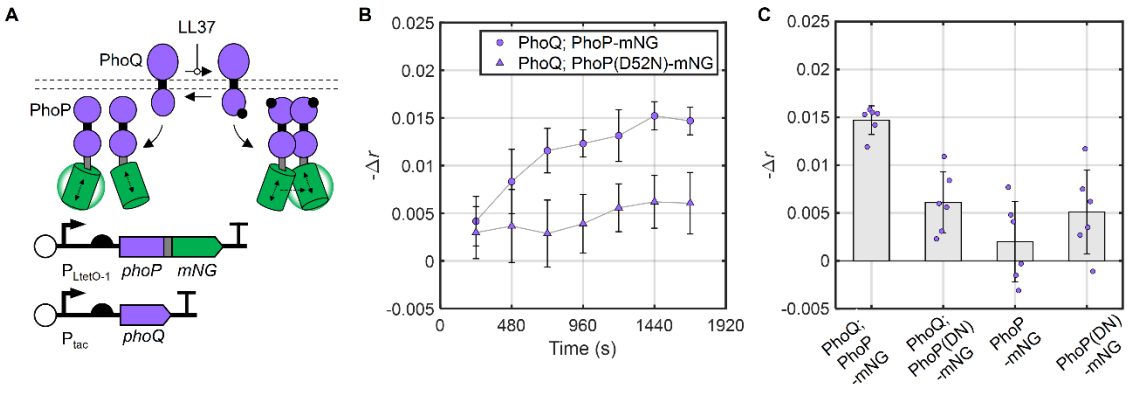

Figure S5: Measuring PhoP dimerization in live bacteria. A. *E. coli* BW30007 (Δ*phoPQ*) was engineered for inducible expression of *S. Typhimurium* PhoQ (IPTG) and PhoP-mNG (aTc) (**Methods**) **B.** Change in anisotropy of cultures treated with the PhoQ activator peptide LL-37 (5 μM) over time. The change in anisotropy is plotted relative to untreated cultures. There is an inherent delay between time zero and the first data point due to manual ligand addition (**Methods**). A control strain expressing PhoP (D52N)-mNG, which cannot be phosphorylated, was constructed and tested. **C.** Change in anisotropy signal of WT (left) and negative control strains treated with LL-37 compared to untreated controls 28 minutes after treatment. (DN) indicates D52N. Cultures were induced with 5.5 ng/mL aTc and 0 μM IPTG in panels B and C. Data represents the mean and standard deviation of two sets of three biological replicates collected on two separate days.

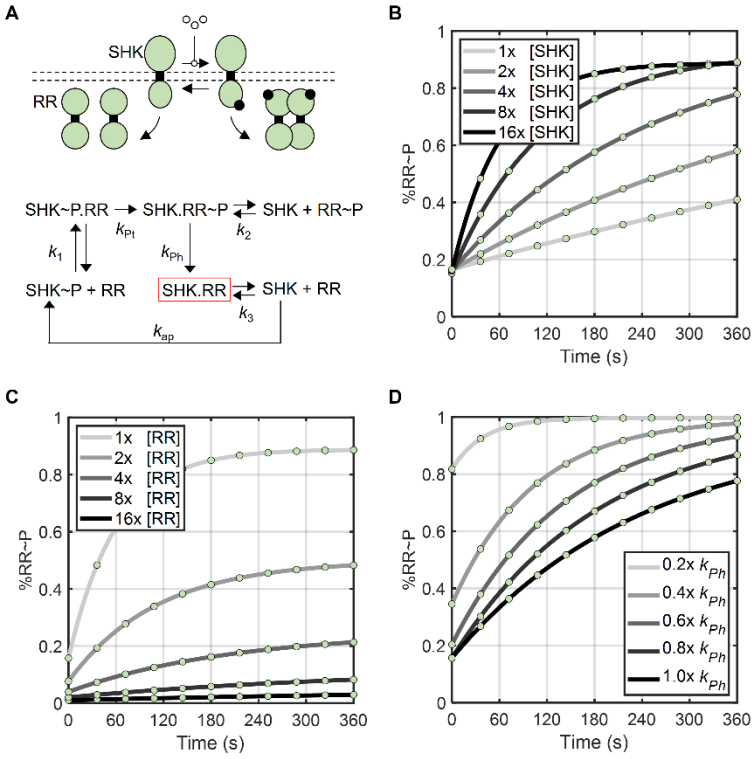

Figure S6. TCS phospho-signaling model. A. Diagram of a generic TCS, and the accompanying model of RR phosphorylation. Reactions and parameters are taken from a previous model that utilized *in vitro* measured parameter values for EnvZ/OmpR (**Table S5**) (6). Red box: dead-end complex. Simulations were equilibrated for 20,000 seconds before the rate of SHK autophosphorylation was switched from 0.05 to 0.3 s^{-1} to represent addition of an activating stimulus. **B.** RR phosphorylation rate as a function of SHK expression level. The fitted $\tau_{1/2}$ values in order of decreasing [SHK] levels (reference SHK concentration 0.017 µM) are 713 s, 353 s, 174 s, 81 s, and 43 s. **C.** RR phosphorylation rate as a function of RR expression level. The fitted $\tau_{1/2}$ values in order of increasing [RR] (reference RR concentration of 6 µM) are 43 s, 78 s, 144 s, 279 s, and 550 s. **D.** RR phosphorylation rate as a function of SHK phosphatase activity. [SHK] and [RR] are fixed at 4x and 1x the reference value, respectively. Fitted $\tau_{1/2}$ values in order of increasing SHK phosphatase (reference SHK phosphatase rate of .05 s^{-1}) are 28 s, 72 s, 100 s, 131 s, and 167 s. Depending on individual TCS parameters, it is possible for decreasing SHK phosphatase activity to both increase the rate and magnitude of RR phosphorylation as seen in our modeling data from 1.0x to 0.6x k_{Ph} (phosphatase rate) as well as in our *in vivo* NarXL data (**Fig. 4**).

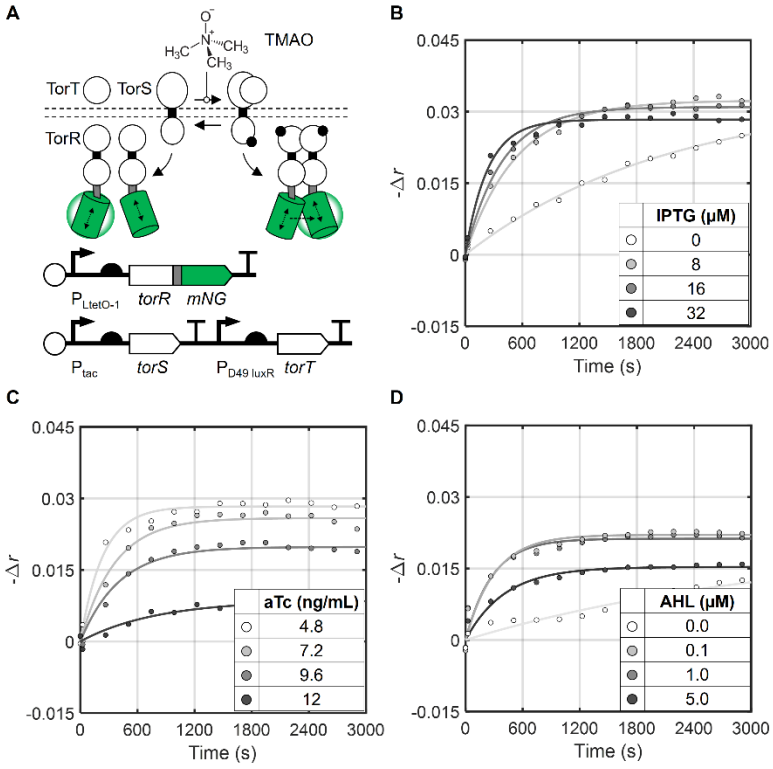

Figure S7. Extended TorR-mNG dimerization time courses. A. Strain diagram. **B.** Anisotropy change over time after TMAO addition (time zero) for cultures induced to express different amounts of TorS (TorR-mNG and TorT induced with 4.8 ng/mL aTc and 1 μM AHL, respectively), **C.** TorR-mNG (TorS and TorT induced with 32 μM IPTG and 1 μM AHL, respectively), or **D.** TorT (TorR and TorS induced with 4.8 ng/mL aTc and 100 μM IPTG, respectively). Data points represent the mean of three biological replicates collected on separate days. Fit lines are first-order exponential functions. Fit parameters are listed in **Table S4**.

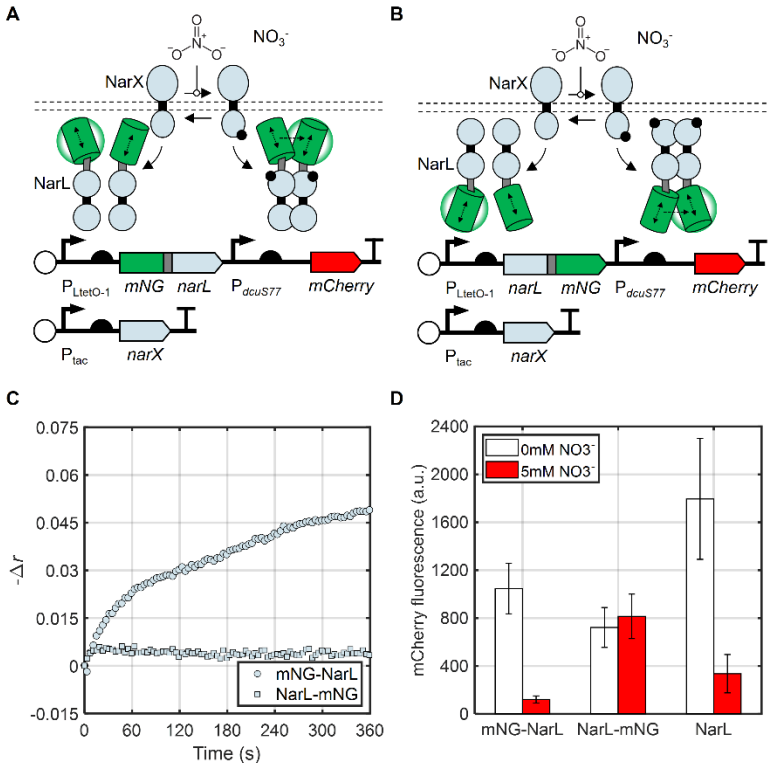

Figure S8. Effect of mNG probe placement on NarL dimerization and transcriptional regulatory activity. Strains engineered to express aTc-inducible (**A**) mNG-NarL and (**B**) NarL-mNG alongside IPTG-inducible NarX and *mCherry* under the control of the NarL-repressible promoter P_{dcuS77}. A control strain expressing WT NarL was also engineered (not shown). **C.** Change in anisotropy over time of each strain after addition of nitrate (time zero). Data points represent the mean of three biological replicates measured on separate days. **D.** P_{dcuS77} transcriptional activity in the absence and presence of nitrate for the strains expressing mNG-NarL, NarL-mNG, and WT NarL. Strains in panels C and D were induced with 4.8 ng/mL aTc and 32 µM IPTG. mCherry expression data are reported as the population mean of segmented-cell median pixel intensities imaged via microscopy (**Methods**). Error bars indicate population standard deviation of segmented-cell median pixel intensities. Roughly 300 cells from two biological replicate populations were imaged for each condition.

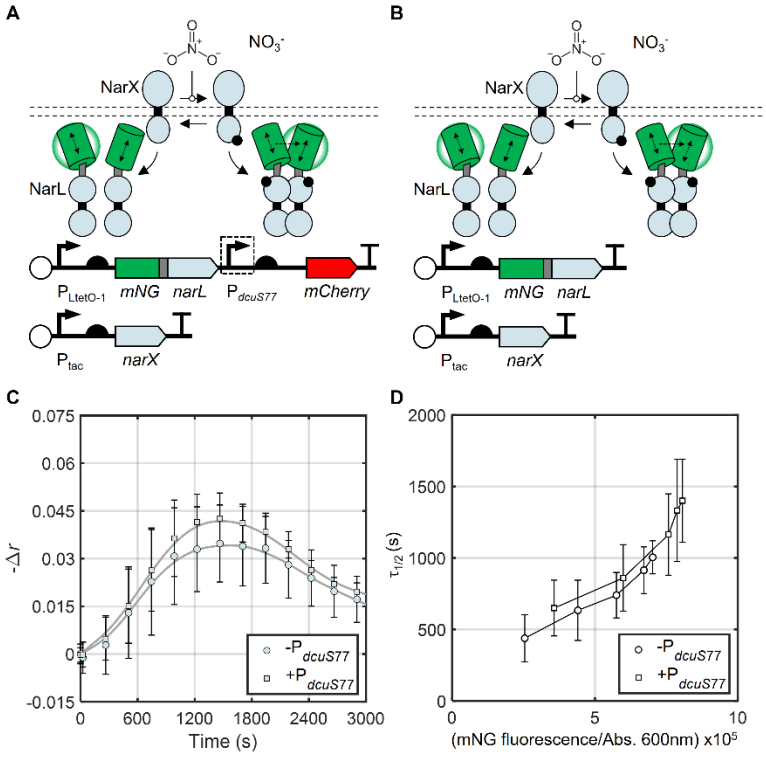

Figure S9: Supplemental NarL target promoters do not affect mNG-NarL dimerization rate. A. Engineered strain for inducible mNG-NarL expression from a ColE1 plasmid backbone with one copy of the NarL-repressed promoter P_{dcuS77} encoded on the plasmid (boxed). **B**. Control strain lacking plasmid-borne P_{dcuS77}. Plasmids are transformed into *E. coli* strain BW29658 (Δ*narXL*), which contains up to 100 NarL-regulated genomic promoters (7) **C.** Anisotropy change over time after nitrate addition (time zero) for cultures with or without P_{dcuS77} present on the plasmid. NarX induced with 100 µM IPTG, mNG-NarL with 6.0 ($-P_{dcuS77}$) or 4.8 ($+P_{dcuS77}$) ng/mL aTc. Smoothing splines were fitted to either data set to guide the eye. **D.** $\tau_{1/2}$ values of mNG-NarL dimerization for different mNG-NarL expression levels in the absence or presence of plasmid-borne P_{dcuS77}. aTc was varied between 4.8 and 9.6 ng/mL as in **Fig. 3D,** NarX was induced by 100 µM IPTG in the presence or absence of plasmid-borne P_{dcuS77}. Data includes three replicates of each condition collected on separate days.

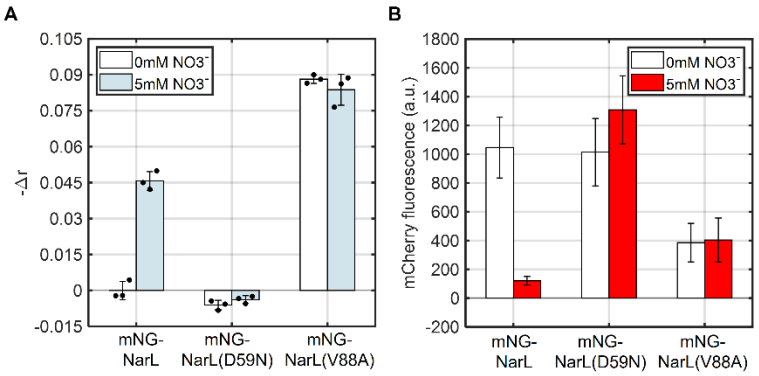

Figure S10. Phosphosignaling mutations validate that mNG-NarL undergoes phosphorylation-dependent dimerization. A. Change in anisotropy signal between 0 and 1,610 seconds following nitrate addition for strains expressing IPTG-inducible NarX and aTc-inducible mNG-NarL, mNG-NarL (D59N), and mNG-NarL (V88A). The D59N mutation renders NarL unable to be phosphorylated while V88A results in phosphorylation-independent NarL activation. Data represent three biological replicates measured on separate days. **B.** Expression of an mCherry transcriptional reporter from P_{dcuS77} after incubation without or with nitrate for 4 h. Cultures in panels A and B were induced with 4.8 ng/mL aTc and 32 µM IPTG. mCherry fluorescence data are reported as the population mean of segmented-cell median pixel intensities imaged via microscopy (**Methods**). Roughly 300 cells from two biological replicate populations were imaged for each condition. Error bars indicate population standard deviation of segmented-cell median pixel intensities.

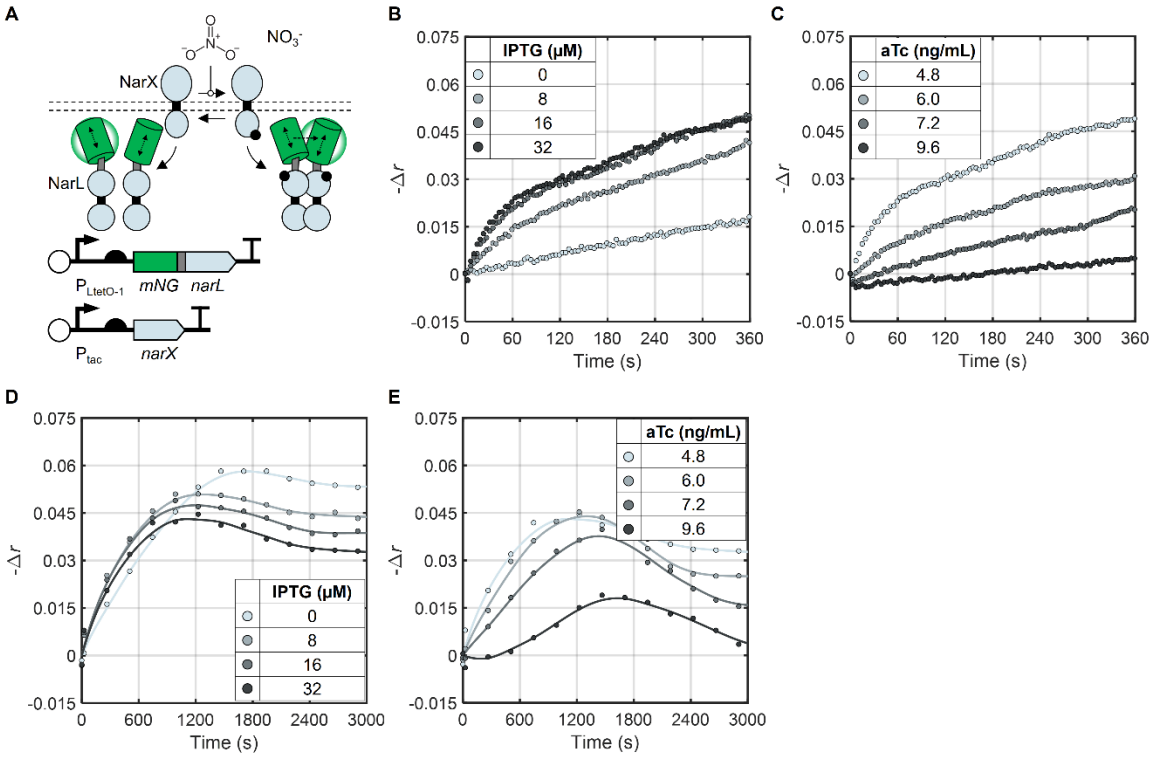

Figure S11. mNG-NarL dimerization time courses. A. Engineered strain for expression of IPTG-inducible NarX and aTc-inducible mNG-NarL. **B-C.** High temporal resolution changes in anisotropy signal over time following nitrate addition (t = 0) of cultures expressing varied amounts of NarX (panel B, mNG-NarL induced with 4.8 ng/mL aTc) or mNG-NarL (panel C, NarX induced with 32 μM IPTG). **D-E.** Longer-term changes in anisotropy signal over time following nitrate addition for cells cultured in the same manner as in panels B-C. Data represent the mean of three biological replicates measured on separate days. Fitted line is a smoothing spline to guide the eye and estimate when peak phosphorylation occurs.

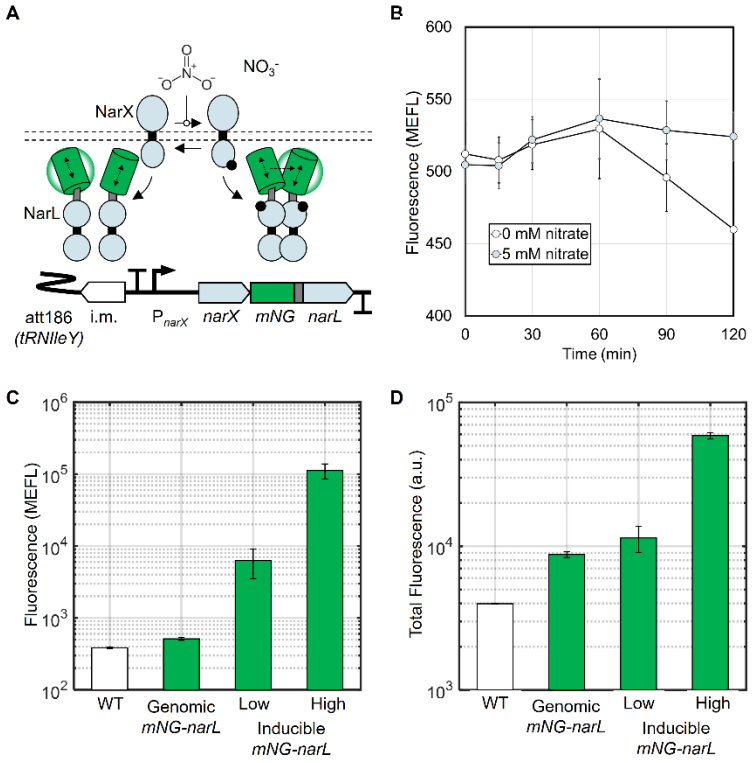

Figure S12: Expression levels of chromosomal- and plasmid-encoded mNG-NarL. A. Engineered strain wherein an *mNG* tag is added to *narL* within the *narXL* operon. To construct this strain, the tagged *narXL* DNA was assembled *in vitro* and cloned into the plasmid pOSIP-KO, which contains an integration module (i.m.) for insertion at the *att186* site within the *tRNIleY* gene (8). The *narX* promoter (P_{narX}) region, comprising 350 base pairs of DNA upstream of *narX*, was included to retain native regulation of the operon. As a result of cloning into pOSIP-KO, the tagged *narXL* operon is flanked by forward and reverse *rrnB* T1 terminators, which insulate it from read-through transcription from adjacent genomic sites (8). This cassette was then integrated into the genome of *E. coli* BW29658 (*ΔnarXL*). **B.** Change in intracellular mNG-NarL over time from the chromosomal system in the absence and presence of nitrate. Data were measured by flow cytometry. Experimental conditions are as in in **Fig. 3E.** mNG-NarL increases during an initial lag phase after the cells are diluted from stationary fresh media. mNG-NarL levels then decrease in the absence of nitrate, presumably due to a lack of autoinduction. The presence of nitrate results in subsequent increases in mNG-NarL levels, presumably due to positive transcriptional autoregulation. Data represent the average median of population fluorescence of nine biological replicates measured on three separate days. Data were collected using flow cytometry. Errors bars represent the standard deviation. **C.** Comparison of mNG-NarL levels expressed from the chromosome (genome) and the plasmid system used throughout this work. 'WT' indicates the parental BW28357 strain, which lacks *mNG*. The genomic system is uninduced by nitrate. 'Low' and 'High' refer to aTc induction at 4 and 10 ng/mL, respectively. These aTc values are the minimum and maximum used for this construct in this work. Bars represent the average median of population fluorescence of three biological replicates measured on a single day, except for the genomic system which represents the same samples at time 0 in panel B. Data were collected using flow cytometry. Errors bars represent the standard deviation. **D.** Plate reader total fluorescence values for cultures and conditions listed in panel C. These data are used for confirming adequate sample fluorescence intensity for anisotropy measurements rather than quantifying single cell mNG-NarL expression levels.

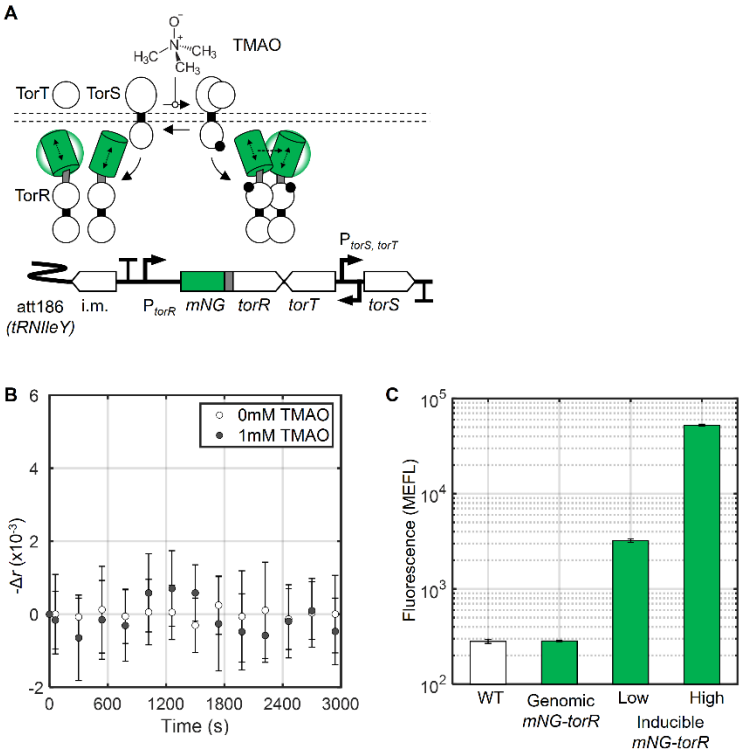

Figure S13: Chromosomal mNG-TorR is expressed below the detection limit. A. Engineered strain wherein an *mNG* tag is added to *torR* within the *torTSR* operon. The strain was constructed as in **Fig. S12**. The *torR* promoter (P_{torR}) region, comprising 350 base pairs of DNA upstream of *torR*, was included to retain native regulation of the operon. The cassette was integrated into the genome of *E. coli* BW29855 (*ΔtorTSRCAD*). **B.** Change in mNG-TorR anisotropy signal over time for bacteria grown in the absence or presence of TMAO. Data were collected and analyzed as in **Fig. S12**. Smoothing spline fits are omitted due to the lack of meaningful signal trends. Data points represent the mean of nine biological replicates collected over three separate days. Error bars indicate the standard deviation. **C.** Comparison of mNG-TorR levels expressed from the genome and the plasmid-expressed mNG-TorR as in **Fig. S12**. 'WT' indicates the parental BW28357 strain, which lacks *mNG*. 'Low' and 'High' refer to aTc induction at 4 and 16 ng/mL, respectively. This induction range fully covers the aTc values used throughout this work. Data were collected using flow cytometry. Bars represent the average arithmetic mean of population fluorescence of three biological replicates measured on a single day. Errors bars represent the standard deviation.

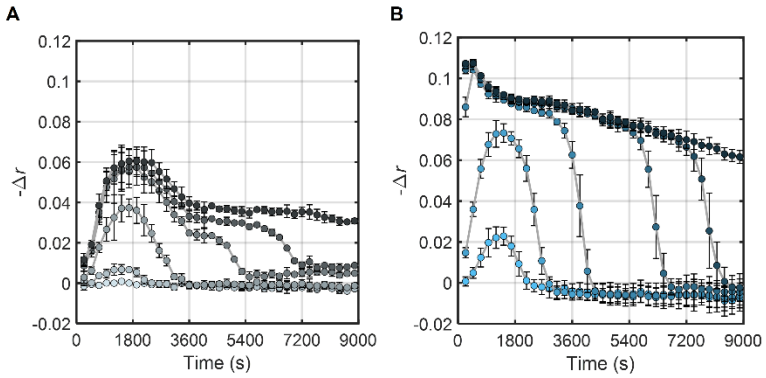

Figure S14: mNG-NarL dimerization overshoot dynamics depend on the supplied nitrate concentration. A. Extended time courses of mNG-NarL dimerization due to NarX-mediated phosphorylation in response to varied concentrations of nitrate (in order of light to dark circles, 1 µM, 10 µM, 100 µM, 500 µM, 1 mM, and 5 mM) added at time zero. **B.** Time courses of mNG-NarL dimerization due to NarX (C415R)-mediated phosphorylation. Nitrate concentrations are the same as panel A. Strains were induced with 4.8 ng/mL aTc and 32 µM IPTG. Data points represent the mean and standard deviation of three biological replicates, subtracted relative to the 0 mM nitrate case for WT NarXL at any given timepoint. Fit lines are smoothing splines to guide the eye.

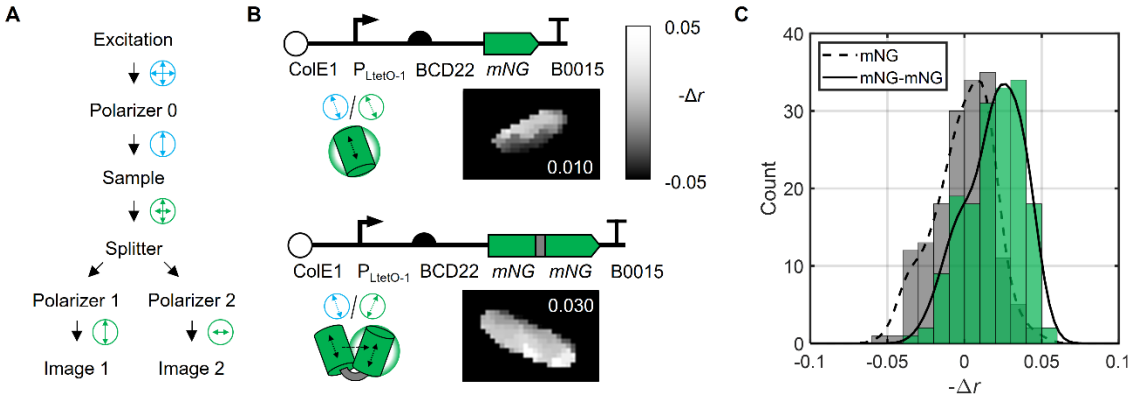

Figure S15: Measuring mNG dimerization in single cells. A. Microscope light path used to obtain parallel and perpendicular fluorescence images in order to calculate fluorescence anisotropy values in single cells. **B.** Genetic diagrams and single-cell images for strains expressing monomeric or dimeric mNG. Image frames are 2.6 x 3.9 µm. **C.** Histograms of single-cell anisotropy signals for strains expressing monomeric or dimeric mNG. All single cell anisotropy values were subtracted by the reference value of the mNG-strain population mean. Separate cultures of each strain were induced with 5 or 7 ng/mL aTc and mixed in order to analyze a wide range of mNG fluorescence values (**Methods**). Approximately 160 cells for each strain were imaged over three separate days. Dashed and dark lines are smoothing splines fit to histogram bin heights to guide the eye.

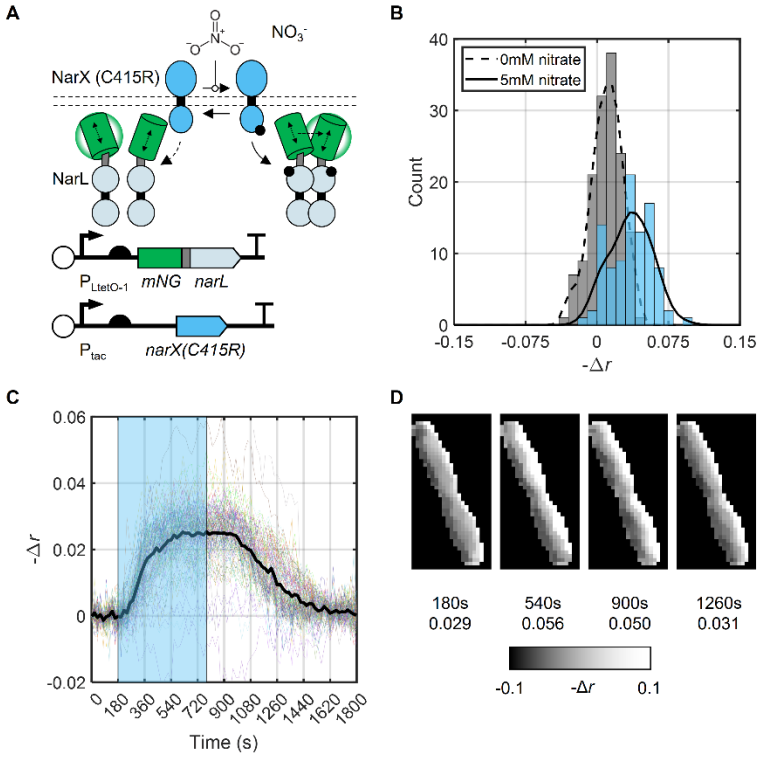

Figure S16: NarL dimerization dynamics in single cells A. Genetic diagram of bacteria engineered to express IPTG-inducible NarX (C415R) and aTc-inducible mNG-NarL. **B.** Histograms of single-cell anisotropy signal values in the absence or presence of nitrate. Approximately 150 cells for each strain were imaged over three separate days. Single-cell anisotropy values are subtracted relative to the mean of cells expressing mNG only (Fig. S13C). **C.** Anisotropy signal over time for single cells exposed to dynamically changing nitrate levels. Thin rainbow-colored lines represent single cell traces that have been linearly detrended based on their respective beginning and ending values. The thick black line represents the average of all single-cell time courses. Blue shading indicates the presence of 5 mM nitrate delivered via a microfluidic device (**Methods**). The plot shows data for 126 cells analyzed on two separate days. There appears to be a delay between nitrate removal and deactivation of the system- further characterization is required to determine if this is truly reflective of NarXL signaling dynamics or caused by slow clearing of nitrate from the microfluidic chamber. **D.** Fluorescence anisotropy image of a single cell before (180 s), during (540 s), and after (900 and 1260 s) stimulation by nitrate. Here the single-cell anisotropy value is reported relative to the mNG-population mean reference value as in panel B. The black background does not indicate an anisotropy signal. NarX and mNG-NarL were induced by 32 μM IPTG and 5.5 ng/mL aTc, respectively.

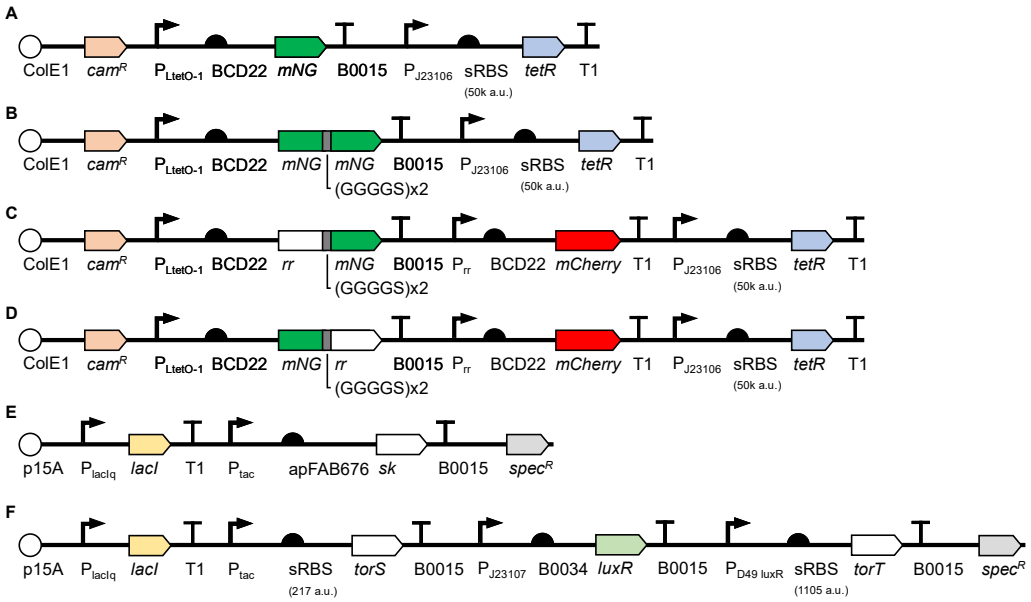

Figure S17: Plasmid schematics. Schematics of plasmids used for inducible expression of **A.** mNG, **B.** mNG-mNG, and **C.** RR-mNG with the *mCherry* transcriptional reporter. P_{rr} refers to the promoter controlled by the relevant RR (P_{dcuS77} for NarL, $P_{torCAD129}$ for TorR). The mCherry reporter is present in all strains used in this study but omitted from main text figures for clarity. Schematics of plasmids used for inducible expression of **D.** mNG-RR, **E**. NarX or PhoQ, and **F.** TorS and TorT.

Table S1. Plasmids used in this study

Plasmid	Purpose	Addgene ID
pRB035	aTc-inducible expression of mNeonGreen	181944
pRB121	aTc-inducible expression of dimerized mNeonGreen (mNG-mNG)	181945
pRB116.2	aTc-inducible expression of TorR with C-terminal mNeonGreen fusion. Also contains mCherry under TorR-controlled promoter PtorCAD129	181946
pRB120.2	aTc-inducible expression of TorR with N-terminal mNeonGreen fusion. Also contains mCherry under TorR-controlled promoter PtorCAD129	181947
pRB113.2	aTc-inducible expression of NarL with C-terminal mNeonGreen fusion. Also contains mCherry under NarL-controlled promoter PdcuS	181948
pRB117.2	aTc-inducible expression of NarL with N-terminal mNeonGreen fusion. Also contains mCherry under NarL-controlled promoter PdcuS	181949
pRB133.2	aTc-inducible expression of PhoP with C-terminal mNeonGreen fusion. Also contains mCherry under PhoP-controlled promoter PvirK	181950
pKD251	IPTG-inducible expression of TorS	124714
pKD317.8	IPTG-inducible expression of NarX	181951
pKB083	IPTG-inducible expression of PhoQ	181952

Table S2. Strains used in this study. Reference corresponding plasmid map in **Fig. S11**.

Strain	**Relevant proteins**	**Plasmid architecture**	**Parent strain**
RB001	mNG	A	BW29658 (Δ*narX, ΔnarL*)
RB002	mNG-mNG	B	BW29658 (Δ*narX, ΔnarL*)
RB003	TorR-mNG, TorS, TorT	C, F	BW29855 (Δ*torR, ΔtorS, ΔtorT*)
RB004	mNG-TorR, TorS, TorT	D, F	BW29855 (Δ*torR, ΔtorS, ΔtorT*)
RB005	TorR-mNG, TorS(H453A), TorT	C, F	BW29855 (Δ*torR, ΔtorS, ΔtorT*)
RB006	TorR(D53N)-mNG, TorS, TorT	C, F	BW29855 (Δ*torR, ΔtorS, ΔtorT*)
RB007	NarL-mNG, NarX	C, E	BW29658 (Δ*narX, ΔnarL*)
RB008	mNG-NarL, NarX	D, E	BW29658 (Δ*narX, ΔnarL*)
RB009	mNG-NarL(D59N), NarX	D, E	BW29658 (Δ*narX, ΔnarL*)
RB010	mNG-NarL, NarX(H399A)	D, E	BW29658 (Δ*narX, ΔnarL*)
RB011	mNG-NarL(V88A), NarX	D, E	BW29658 (Δ*narX, ΔnarL*)
RB012	mNG-NarL, NarX(C415R)	D, E	BW29658 (Δ*narX, ΔnarL*)
RB013	PhoP-mNG, PhoQ	C, E	BW3007 (Δ*phoQ, ΔphoP*)
RB014	PhoP(D52N)-mNG, PhoQ	C, E	BW3007 (Δ*phoQ, ΔphoP*)
RB015	PhoP-mNG	C	BW3007 (Δ*phoQ, ΔphoP*)
RB016	PhoP(D52N)-mNG	C	BW3007 (Δ*phoQ, ΔphoP*)
RB017	mNG-NarL, NarX	Genomically-integrated (Fig. S15A, Methods)	BW29658 (Δ*narX, ΔnarL*)

Table S3. Typical absolute anisotropy (*r*) values for various samples examined in this work. Error describes standard deviation of three biological replicates. Peak values are used for the NarXL data.

Sample	Unstimulated *r*	Stimulated *r*
mNG	0.3095 ± 0.0017	
mNG-mNG	0.2711 ± 0.0043	
TorS, mNG-TorR	0.2641 ± 0.0029	0.2372 ± 0.0033
TorS, TorR-mNG	0.2865 ± 0.0032	0.2546 ± 0.0083
TorS (H453A), TorR-mNG	0.2941 ± 0.0023	0.2920 ± 0.0063
TorS, TorR (D53N)-mNG	0.2963 ± 0.0036	0.2949 ± 0.0058
NarX, NarL-mNG	0.3012 ± 0.0061	0.2525 ± 0.0099
NarX, mNG-NarL	0.3104 ± 0.0038	0.2647 ± 0.0039
NarX (H399A), mNG-NarL	0.3202 ± 0.0032	0.3247 ± 0.0043
NarX, mNG-NarL (D59N)	0.3142 ± 0.0016	0.3165 ± 0.0020
NarX, mNG-NarL (V88A)	0.2266 ± 0.0065	0.2222 ± 0.0018
NarX (C415R), mNG-NarL	0.3111 ± 0.0056	0.2195 ± 0.0022
Genomic NarX, mNG-NarL	0.0674 ± 0.0017	0.0646 ± 0.0018

Table S4. Data fit parameters.

1st order exponential systems (Eq. 2) TorS, TorR-mNG	**a (95% confidence bounds)**	**b (95% confidence bounds)**	**c (95% confidence bounds)**
0 µM IPTG, 4.8 ng/mL aTc	0.03351 (0.03848, 0.02854)	-0.000468 (-0.000603, -0.000332)	0.0010 (-0.0042 0.0063)
8 µM IPTG, 4.8 ng/mL aTc	0.03234 (0.03386, 0.03082)	-0.001866 (-0.002123, -0.001609)	0.0007 (-0.0002 0.0017)
16 µM IPTG, 4.8 ng/mL aTc	0.03096 (0.03227, 0.02966)	-0.002574 (-0.002905, -0.002243)	0.0006 (-0.0001 0.0013)
32 µM IPTG, 4.8 ng/mL aTc	0.02831 (0.02993, 0.0267)	-0.004243 (-0.00511, -0.003377)	0.0004 (-0.0003 0.0012
32 µM IPTG, 7.2 ng/mL aTc	0.02794 (0.03045, 0.02544)	-0.002982 (-0.003828, -0.002137)	-0.0014 (-0.0026 -0.0000)
32 µM IPTG, 9.6 ng/mL aTc	0.01982 (0.02185, 0.01779)	-0.002465 (-0.003228, -0.001701)	-0.0012 (-0.0023 -0.0001)
32 µM IPTG, 12 ng/mL aTc	0.008653 (0.01014, 0.00716)	-0.001257 (-0.001887, 0.0006282)	-0.0012 (-0.0024 0.0001)
Smoothing Spline NarX, mNG-NarL	**Est. peak**	**Est. $\tau_{1/2}$ (s)**	
0 µM IPTG, 4.8 ng/mL aTc	0.0581	561	
8 µM IPTG, 4.8 ng/mL aTc	0.0509	307	
16 µM IPTG, 4.8 ng/mL aTc	0.0474	279	
32 µM IPTG, 4.8 ng/mL aTc	0.0439	285	
32 µM IPTG, 6.0 ng/mL aTc	0.0439	399	
32 µM IPTG, 7.2 ng/mL aTc	0.0376	537	
32 µM IPTG, 9.0 ng/mL aTc	0.0180	933	
NarX (C415R), mNG-NarL 32 µM IPTG, 4.8 ng/mL aTc	0.0823	28	
Hill function fit (Eq. 3)	**a (95% confidence bounds)**	**b (95% confidence bounds)**	
NarX, mNG-NarL dose response	1.181 (1.088, 1.274)	0.03739 (0.02787, 0.04691)	
NarX (C415R), mNG-NarL dose response	1.282 (1.196, 1.368)	0.000849 (0.0004508, 0.001247)	

Table S5. TCS modeling parameters, adapted from a previous computational study (6). Default values are bolded

Parameter	Value	Description
k_{ap}	0.05 s^{-1} (inactive), 0.30 s^{-1} (active)	SHK autophosphorylation
k_{ad}	0.001 s^{-1}	SHK autodephosphorylation
k_1	0.5 μM s^{-1}	Reversible formation of SHK~P.RR complex
k_2	0.5 μM s^{-1}	Reversible formation of SHK.RR~P complex
k_3	0.5 μM s^{-1}	Reversible formation of SHK.RR complex
k_{Pt}	1.5 s^{-1}	SHK kinase rate
k_{ph}	**0.05**, 0.04, 0.03, 0.02, and 0.01 s^{-1}	SHK phosphatase rate
[RR]	**6**, 12, 24, 48, and 96 μM	Total available RR concentration
[SHK]	**0.017**, 0.034, 0.068, 0.136, and 0.272 μM	Total available SHK concentration

SI References

1. K. Stevenson, A. F. McVey, I. B. N. Clark, P. S. Swain, T. Pilizota, General calibration of microbial growth in microplate readers. *Scientific Reports* **6** (2016).
2. M. D. Hall, *et al.*, Fluorescence polarization assays in high-throughput screening and drug discovery: A review. *Methods and Applications in Fluorescence* **4** (2016).
3. N. C. Shaner, *et al.*, A bright monomeric green fluorescent protein derived from Branchiostoma lanceolatum. *Nature Methods* **10**, 407–409 (2013).
4. A. N. Bader, E. G. Hofman, J. Voortman, P. M. P. van Bergen En Henegouwen, H. C. Gerritsen, Homo-FRET imaging enables quantification of protein cluster sizes with subcellular resolution. *Biophysical Journal* **97**, 2613–2622 (2009).
5. B. Shao, *et al.*, Single-cell measurement of plasmid copy number and promoter activity. *Nature Communications* **12**, 1475 (2021).
6. O. A. Igoshin, R. Alves, M. A. Savageau, Hysteretic and graded responses in bacterial two-component signal transduction. *Molecular Microbiology* **68**, 1196–1215 (2008).
7. C. Constantinidou, *et al.*, A reassessment of the FNR regulon and transcriptomic analysis of the effects of nitrate, nitrite, NarXL, and NarQP as Escherichia coli K12 adapts from aerobic to anaerobic growth. *Journal of Biological Chemistry* **281**, 4802–4815 (2006).
8. F. St-Pierre, *et al.*, One-Step Cloning and Chromosomal Integration of DNA. *ACS Synthetic Biology* **2**, 537–541 (2013).